Deep–Sea Research I 226 (2025) 104605

Contents lists available at ScienceDirect

Deep-Sea Research Part I

journal homepage: www.elsevier.com/locate/dsri

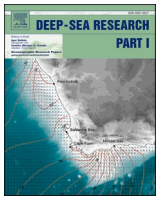

Latitudinal transitions of eddy-affected zooplankton abundance in the mid-latitude North Atlantic

Guiyan Han [a,b,c,e], Graham D. Quartly [c], Hui Wang [a,e,*], Jie Yang [b,d], Ge Chen [b,d]

[a] Institute of Marine Science and Technology, Shandong University, Qingdao, 266237, China
[b] State Key Laboratory of Physical Oceanography, Department of Marine Technology, Ocean University of China, Qingdao, 266100, China
[c] Plymouth Marine Laboratory, Prospect Place, The Hoe, Devon, Plymouth, PL1 3DH, United Kingdom
[d] Laboratory for Regional Oceanography and Numerical Modeling, Department of Ocean Big Data and Prediction, Laoshan Laboratory, Qingdao, 266237, China
[e] Shandong Key Laboratory of Intelligent Marine Engineering Geology, Environment and Equipment, Qingdao, 266237, China

ARTICLE INFO

Keywords:
Mesoscale eddies
Zooplankton abundance
North Atlantic
Chlorophyll
Sea surface temperature

ABSTRACT

Mesoscale eddies play a critical role in marine ecosystems by regulating ocean environments and thereby influencing marine life. By integrating zooplankton observations from the Continuous Plankton Recorder (CPR) project with satellite-derived sea surface temperature (SST), chlorophyll (Chl) concentration, and eddy datasets based on sea surface height, we investigate the impacts of eddy populations on zooplankton community abundance in the North Atlantic. To comprehensively assess both the abundance and richness of zooplankton communities, we introduced the Abundance Index as a unifying metric. The mid-latitude North Atlantic is segmented into three latitudinal zones: the southern zone (35°N–45°N), the middle zone (45°N–55°N), and the northern zone (55°N–70°N). Our analysis revealed distinct annual variations in the Abundance Index across the three zones from 1993 to 2017. The Abundance Index was consistently higher within cyclonic eddy (CE) cores compared with anticyclonic eddy (AE) cores in the southern and northern zones, contrasting with the patterns in the middle zone. However, the composite patterns of eddy-affected Chl and SST were similar across all zones. By employing six machine learning models, we assessed the feature importance (*FI*) of log-transformed Chl (log-Chl) and SST in explaining the Abundance Index. Log-Chl was found to have a greater impact than SST, particularly in the northern zone, highlighting the greater importance of food availability relative to ambient temperature. Significant shifts in the Abundance Index differences between AE and CE cores were detected in 1998, 2002, and 2003 in the southern, middle, and northern zones, respectively, suggesting that optimal habitats may have shifted in response to ocean climate change. These findings provide deeper insights into the effects of mesoscale eddies on zooplankton communities and highlight their broader implications for marine ecosystem dynamics.

1. Introduction

Mesoscale eddies are ubiquitous rotating water masses in the oceanic realm, representing a prominent oceanographic phenomenon characterized by spatial scales spanning tens to hundreds of kilometers and temporal durations ranging from several days to years (Chelton et al., 2011a, 2011b). The dynamic processes inherent in these eddies generate unique physical, chemical, and biological attributes that set them apart from the surrounding waters. Zooplankton—key intermediaries in marine food webs—are particularly susceptible due to their limited mobility. Through essential behaviors such as respiration, grazing, excretion, and diel vertical migration (DVM), zooplankton facilitate the transfer of energy from primary producers to fish populations (Benedetti et al., 2021; Govoni et al., 2010), and thus play a significant role in global biogeochemical cycles (Eden et al., 2009).

Mesoscale eddies influence zooplankton communities through both horizontal and vertical dynamic processes. Horizontally, eddies can transport or redistribute phytoplankton (Chelton et al., 2011a; Gaube et al., 2014) and have the capacity to trap zooplankton (Durán-Campos et al., 2015; Govoni et al., 2010; Zhu et al., 2009). Vertically, eddy dynamics can induce upwelling or downwelling and displace isopycnal surfaces (Gaube et al., 2014; McGillicuddy, 2016), thereby altering light

* Corresponding author. Institute of Marine Science and Technology, Shandong University, Qingdao, 266237, China.
E-mail address: wangh@nmefc.cn (H. Wang).

https://doi.org/10.1016/j.dsr.2025.104605
Received 8 January 2025; Received in revised form 12 September 2025; Accepted 13 October 2025
Available online 17 October 2025

conditions, temperature, ocean mixing, and nutrient availability (Falkowski et al., 1991; Gaube et al., 2015; McGillicuddy et al., 2007). These changes subsequently affect phytoplankton growth and a range of zooplankton characteristics, including distribution (Batten and Crawford, 2005; Govoni et al., 2010), abundance (Eden et al., 2009; Strzelecki et al., 2007; Wang et al., 2023), biomass (Govoni et al., 2010; Labat et al., 2009; McGillicuddy et al., 2007), behavior (Eden et al., 2009), community structure (Durán-Campos et al., 2015; Eden et al., 2009), and grazing rate (An et al., 2024). These effects can propagate to higher trophic levels, influencing the behavior of tropical predators (Xing et al., 2023, 2024).

Although previous case studies have identified associations between the behavior of specific zooplankton species and mesoscale eddies, notable limitations persist. Most investigations have concentrated on a narrow set of taxa, leading to insufficient taxonomic coverage and an absence of a comprehensive community-level perspective. Furthermore, the prevalent reliance on site-based observations has constrained both the spatial and temporal resolution of findings, thereby hindering the detection of broad-scale response patterns. Systematic cross-regional assessments of entire zooplankton communities, along with the mechanisms underlying their responses to mesoscale eddies, remain scarce. It is still unclear whether these responses are primarily governed by temperature-driven physiological processes (An et al., 2024; Wang et al., 2023), such as metabolic rate changes, or by bottom-up regulation in which food availability (Liu et al., 2020)—typically represented by chlorophyll (Chl)—plays the driving role. Clarifying these issues is essential for advancing our understanding of the mesoscale physical–biological interactions in marine ecosystems.

To address these gaps, this study investigates latitudinal variations in zooplankton abundance and vertical behavior in relation to mesoscale eddies across the mid-latitude North Atlantic (35°–70°N). This region is chosen because of the abundance of quantitative zooplankton data from historical surveys by the Continuous Plankton Recorder (CPR). Fig. 1 shows the frequent surveys along the key trade routes from the United Kingdom to North America, including via Iceland. We combine these observations with satellite-derived eddy datasets of sea surface temperature (SST) and Chl data, and machine learning approaches to explore how eddy polarity, eddy region, and physical-biological factors jointly influence zooplankton abundance. We hypothesize that the regions outside eddies (see section 2.3) are minimally affected by eddy dynamics and can therefore serve as a reference baseline. To explain the impacts of eddies on zooplankton, we propose two competing hypotheses: (1) the temperature-driven hypothesis, which posits that environmental temperature has a stronger influence on zooplankton dynamics (An et al., 2024; Wang et al., 2023), and (2) the food-driven hypothesis, which argues that food availability, represented by Chl concentration, exerts the greater control (Liu et al., 2020). Through the observed findings and these two hypotheses, we aim to advance our understanding of the long-term dynamics of zooplankton communities under the influence of mesoscale eddies and to clarify the roles of key drivers in shaping these interactions.

2. Materials and methods

2.1. Data

Sea level anomaly (SLA): The SLA data were from multiple altimeter missions processed by AVISO (AVISO, 2019), including TOPEX/-Poseidon, ERS-1/2, ENVISAT, JASON-1/2/3, Sentinel-3A, HY-2A, Saral/AltiKa, Cryosat2, and GFO. We used the daily "all-satellite" SLA dataset on a ¼° longitude-latitude grid, which integrates observations from all available altimeters. In addition, the AVISO two-satellite product is based solely on missions operating on the 10-day and 35-day (or 27-day) sampling patterns (see Fig. 1 of Quartly et al. (2017)), which provide homogeneous spatial coverage throughout the analysis period. This product was used to check the consistency of eddy tracking in the "all-satellite" dataset.

Continuous Plankton Recorder: Initiated in 1931, the CPR survey represents the world's longest-running and largest multi-decadal plankton monitoring program (Piontkovski et al., 1995; Johns and Broughton, 2022). A CPR is towed at approximately 7 m depth behind vessels traveling at 15–20 knots. Each device funnels water onto a slowly and constantly rotating strip of silk, filtering all particulates larger than the mesh size of 270 μm. After each transect, the silk is cut into individual 0.1 m segments, each representing plankton collected over 18 km (10 nautical miles) of tow, corresponding to the filtration of approximately 3 m^3 of seawater (Piontkovski et al., 1995). The samples undergo four separate stages of analysis: (1) overall Chl, (2) larger phytoplankton cells, (3) small zooplankton (<2 mm), and (4) large zooplankton (≥2 mm). Large zooplankton (referred to as "Eye-count") are individually removed from the silk and identified visually, whereas for small zooplankton (referred to as Traverse-count), a representative series of traverses covering 2 % of the silk are undertaken with a high-performance microscope, thus the expected total number is estimated by multiplying by 50. Although CPR-derived estimates are semi-quantitative in nature, they still provide robust and long-term insights into changes in zooplankton abundance (Piontkovski et al., 1995).

Sea surface temperature: The Optimum Interpolation Sea Surface Temperature (OI-SST) products, spanning January 1, 1998, to December 31, 2017, were obtained from NOAA. These daily products have a spatial resolution of 25 km and are derived exclusively from AVHRR observations.

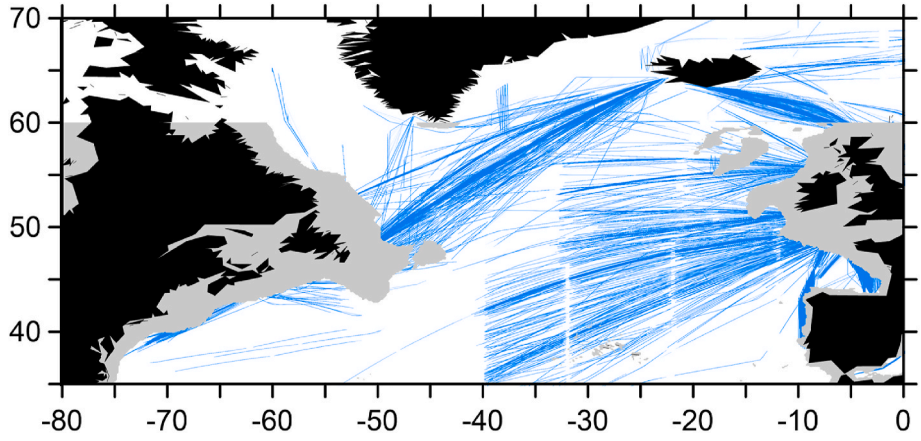

Fig. 1. CPR tracks in the mid-latitude North Atlantic during 1993–2017. Each line segment represents a section of the CPR tow identified by its own unique event ID. Regions of water depth shallower than 1000 m are shaded in grey.

Chlorophyll concentration: The Chl data were obtained from the GlobColour project, funded by the European Space Agency. The dataset combines SeaWiFS observations from January 1, 1998, to June 22, 2002, with MODIS/VIIRS data from June 23, 2002, to December 31, 2017. Daily products were generated using the Garver–Siegel–Maritorena (GSM) algorithm at a spatial resolution of 25 km. Because Chl typically exhibits a log-normal distribution (Campbell, 1995; Chelton et al., 2011b), all values were log-transformed (base 10, log-Chl) prior to analysis.

Data selection and preprocessing: To ensure spatiotemporal consistency across datasets, this study focuses on the mid-latitude North Atlantic (35°N–70°N) for the period from January 1, 1998, to December 31, 2017. The core analysis uses CPR data from March to August each year, with additional data from April to October employed to assess the robustness of results within the 45°–55°N band (see details in Text S1). All statistical analyses applied after a two-standard-deviation outlier removal procedure to enhance robustness.

2.2. CPR data processing

2.2.1. The Abundance Index

Zooplankton counts from the CPR were standardized by dividing by the volume of filtered water (3 m^3) and log-transformed using $\log_{10}(x+1)$ to reduce variability and allow for abundance differences between small and large species (Rettig, 2003). To capture both abundance and species diversity, we introduced an ***Abundance Index*** as a composite metric of zooplankton community structure, defined as follows:

$$\text{Abundance Index} = \sum_{i=1}^{i=n} log_{10}\left(\frac{x_i}{3}+1\right) \tag{1}$$

where n denotes the total number of zooplankton taxa observed, x represents the individual count for each taxon, and the division by 3 normalizes the values by the volume of filtered water. We also considered three other metrics commonly used in zooplankton research: Abundance (An et al., 2024), Diversity and Richness (Lu et al., 2022).

$$\text{Abundance} = log_{10}\left(\sum_{i=1}^{i=n}\frac{x_i}{3}+1\right) \tag{2}$$

$$\text{Diversity} = -\sum_{i=1}^{i=n} P_i \cdot \ln P_i \tag{3}$$

$$\text{Richness} = n \tag{4}$$

where P denotes the numerical proportion of a given taxon.

2.2.2. N:D ratio of zooplankton

The nighttime-to-daytime (N:D) ratio was introduced as an indicator to evaluate zooplankton DVM response to mesoscale eddies. Following the method of Behrenfeld et al. (2019), local sunrise and sunset times were estimated for each CPR observation based on its date and geographic coordinates. These times were converted to UTC to match the CPR sampling timestamps, allowing observations to be classified as either daytime or nighttime. The N:D value is defined as the ratio of the nighttime to daytime Abundance Index:

$$N:D = \frac{\textit{Abundance Index for Nighttime}}{\textit{Abundance Index for Daytime}} \tag{5}$$

2.2.3. Significance test

To evaluate differences between two zooplankton groups, the normality of each group was assessed using the D'Agostino and Pearson test. If both groups met the normality assumption ($p > 0.05$), an independent two-sample t-test was conducted; otherwise, the non-parametric Mann–Whitney U test was applied. All statistical analyses were conducted in Python with the SciPy library, and significance was determined at $p < 0.05$.

Pearson correlation coefficients were calculated to evaluate associations between two data groups. Prior to analysis, the data were examined for approximate normality and outliers. Statistical significance was assessed using two-tailed p-values derived from t-tests associated with the Pearson correlation (r), implemented via the 'pearsonr' function in the Python SciPy library. A significance level of $p < 0.05$ was applied.

2.3. Eddy processing framework

2.3.1. Eddy identification and tracking

Based on the improved eddy identification and tracking methods of Tian et al. (2020), an eddy dataset for the North Atlantic was created. For eddy identification, global SLA fields were first high-pass filtered using a half-power Gaussian filter to determine eddy seed points effectively (local maxima or minima). SLA contours were then generated at 0.25-cm intervals. The closed SLA contour with the maximum average geostrophic current speed was defined as the eddy boundary, provided it enclosed no more than one seed point. For tracking, each eddy identified on Day 1 was matched with eddies of the same polarity (i.e. AE or CE) occurring within 0.5° of its centroid on the following day. If multiple candidates were found, the target eddy was determined based on a set of similarity parameters (kinetic energy, distance, amplitude, and area), normalized by globally derived characteristic values.

To be confident that we had robust identification of mesoscale eddies, only those with lifetimes longer than 10 days were retained for further analysis. Additionally, eddies were only considered if their SLA magnitude exceeded 1 cm, their boundary encompassed at least 8 grid points (0.25° apart), and they existed in a water depth of at least 1000 m. Most eddies in the Gulf Stream have lifetimes shorter than 10 days, thus leading to fewer trackable eddies identified in the Gulf Stream.

2.3.2. Matching observations with eddies

From 1993 to 2017, more than 2000 individual eddies with lifetimes longer than 10 days were selected for analysis. The CPR data, along with satellite observations of SST and Chl, were viewed in the context of their position within the eddy field, considering the polarity of the eddies (i.e. cyclonic or anticyclonic) and the relative radius (Rr) of each observation. The Rr ranged from zero at the eddy centroid, one at the eddy boundary, to two at twice the distance from the eddy centroid. Eddy regions were defined as follows: from 0 to 0.8 as the eddy core, from 0.8 to 1.2 as the eddy edge, and from 1.2 to 2.0 as outside the eddy region (Xiu and Chai, 2020). We expect observations in the outside-eddy region to be unaffected by the eddy dynamics and thus provide a measure of the background features, serving as a baseline to assess the influence of eddy dynamics.

2.3.3. Eddy-induced anomalies of observations

Assuming that regions outside eddies are unaffected by eddy activity, eddy-induced anomalies in the Abundance Index are defined as the differences between eddy cores and surrounding non-eddy regions. These anomalies were then used to analyze the long-term temporal variations of the Abundance Index. This process mitigates statistical bias arising from the uneven spatiotemporal distribution of CPR–eddy matchups and highlights the regulatory role of mesoscale eddies on zooplankton relative to the surrounding marine environment.

2.4. Using machine learning for zooplankton regression

Machine learning regression methods are well-suited for capturing nonlinear and complex relationships within data. Some regressors also provide feature importance (*FI*) indices, which offer an intuitive way of evaluating the relative influence of different factors on the target variable. In Section 3.7, we employ six machine learning

algorithms—Decision Tree, Random Forest, Extra Trees, Gradient Boosting, Light Gradient Boosting Machine, and Categorical Boosting—to assess the relative importance of SST and log-Chl in shaping zooplankton abundance. Regression models were constructed using SST, log-Chl, longitude, latitude, year, and day of the year as predictors. All six models return the 'feature_importances_' attribute in Python, enabling direct comparison of SST and log-Chl contributions across different modeling approaches.

Among these machine learning algorithms, the *FI* scores produced by Decision Tree, Random Forest, Extra Trees, and Gradient Boosting models sum to one, whereas those from Categorical Boosting sum to 100, and those from Light Gradient Boosting Machine are expressed on a non-comparable scale. To ensure consistency across models, we normalized the *FI* scores for SST and log-Chl using the following formula:

$$FI_{SST} = \frac{FI_{SST'}}{FI_{SST'} + FI_{Chl'}} \quad (5)$$

$$FI_{Chl} = \frac{FI_{Chl'}}{FI_{SST'} + FI_{Chl'}} \quad (6)$$

where FI_{SST} and FI_{Chl} represent the normalized *FI* of SST and log-Chl, and $FI_{SST'}$ and $FI_{Chl'}$ denote the raw *FI* values output by Python. To reduce the undue influence of individual algorithms on the assessment, quality control was performed on the normalized *FI* scores by excluding data that exceeded two standard deviations from the mean. The final *FI* estimates for SST (FI_{SST}) and log-Chl (FI_{Chl}) were then obtained by averaging the remaining scores.

3. Results

3.1. Study regions and their key environmental characteristics

Our study examines the mid-latitude North Atlantic, spanning from 35°N to 70°N. Fig. 2 illustrates the physical, dynamic, and biological characteristics of this region, along with the distributions of CPR samples and mesoscale eddies. Surface waters are marked by high Chl concentrations, with coastal areas displaying substantially higher levels than the open ocean (Fig. 2a). SST isotherms closely trace the coastline of North America and Greenland, while other regions exhibit a general northward gradient (Fig. 2b). The northeastern North Atlantic hosts a greater number of eddies with lifetimes exceeding 10 days (Fig. 2c), whereas the Gulf Stream region exhibits the highest eddy kinetic energy (EKE) (Fig. 2d). Areas of elevated EKE typically correspond to fewer detected eddies and CPR samples, whereas regions with more uniform CPR coverage generally coincide with lower EKE (Fig. 2c–e).

We found that zooplankton responses to mesoscale eddies vary across different latitudinal zones. Accordingly, the mid-latitude North Atlantic (35°N–70°N) was divided into three distinct zones, primarily based on observed differences in zooplankton Abundance Index between eddy polarities. Table 1 summarizes the Abundance Index within the cores of the AE and CE, which are more pronounced than those at the eddy edges and outside the eddies (see Table S1). In addition, Table 1 reports the mean SST and log-Chl values for each 5° latitudinal zone across the study area. The three latitudinal zones were defined as follows:

- Southern zone (35°N–45°N): The Abundance Index is significantly higher within CE cores than within AE cores (Table 1, $p < 0.01$).
- Middle zone (45°N–55°N): The Abundance Index is higher within AE cores than within CE cores, with significant differences observed from April to October (Table 1 and Table S1, $p < 0.01$).

Table 1
Averages of latitudinal log-Chl, SST and Abundance Index from March to August.

Latitudinal Zones		Abundance Index		*p*	Log-Chl ($mg \cdot m^3$)	SST (°C)
		AE cores	CE cores			
Southern Zone	35°N–40°N	5.13	6.37	<0.01	−0.88	20.34
	40°N–45°N	5.91	6.76		−0.60	16.57
Middle Zone	45°N–50°N	7.25	6.98	0.07	−0.42	13.82
	50°N–55°N	7.31	7.07		−0.31	10.70
Northern Zone	55°N–60°N	7.09	7.37	<0.001	−0.34	8.16
	60°N–65°N	5.82	7.47		−0.26	6.96
	65°N–70°N	7.82	12.14		−0.28	2.24

*p represents the significance level of the difference in abundance between AE and CE cores.

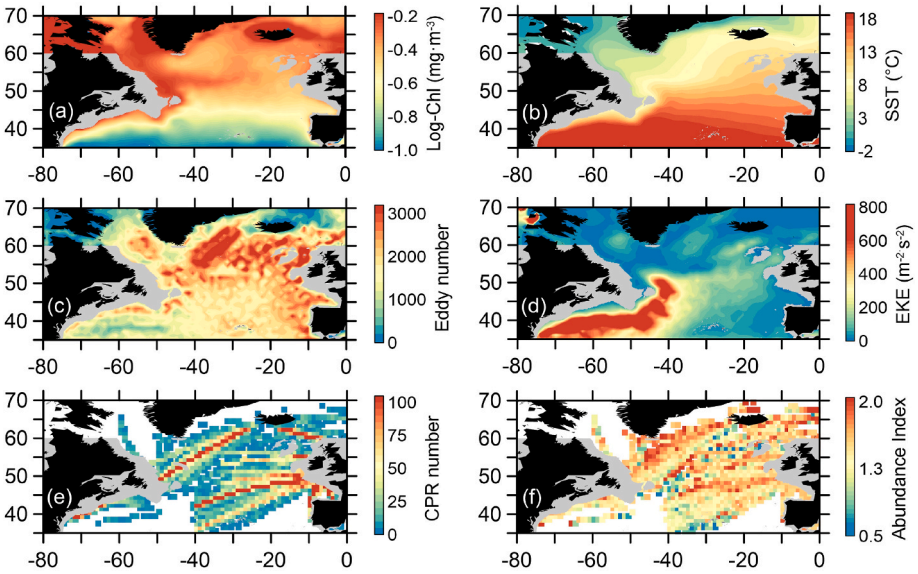

Fig. 2. Physical, dynamic, and biological features of the mid-latitude North Atlantic. The subplots show the distributions of the mean (a) log-Chl, (b) SST, (c) eddy number, (d) EKE, (e) number of CPR samples located within twice eddy boundaries, and (f) Abundance Index. The maps are plotted on a 1° grid, with regions of water depth shallower than 1000 m are shaded in grey.

- Northern zone (55°N–70°N): The Abundance Index is significantly higher within CE cores than within AE cores (Table 1, $p < 0.001$).

3.2. Abundance Index with conventional metrics

Based on approximately 44,000 samples, the Abundance Index exhibited strong positive correlations with total abundance ($r = 0.93$, $p < 0.001$), diversity ($r = 0.76$, $p < 0.001$), and richness ($r = 0.86$, $p < 0.001$). In contrast, total abundance showed relatively weaker correlations with diversity ($r = 0.55$, $p < 0.001$) and richness ($r = 0.64$, $p < 0.001$). The fitted relationships between the Abundance Index and ecological metrics are presented in Fig. 3. The Abundance Index showed a significant logarithmic relationship with total abundance ($R^2 = 0.84$, $p < 0.001$), and significant linear relationships with diversity ($R^2 = 0.83$, $p < 0.001$) and richness ($R^2 = 0.89$, $p < 0.001$). In comparison, the traditional metrics Diversity and Richness were strongly correlated with each other ($R^2 = 0.85$, $p < 0.001$). However, both linear and logarithmic relationships between Diversity and Abundance were weak, with R^2 values below 0.1 (not shown).

3.3. Monthly variations in Abundance Index and CPR sampling

The Abundance Index and CPR sample numbers exhibited pronounced seasonal patterns (Fig. 4), driven by seasonal variability in zooplankton DVM, the CPR sampling schedule, and mesoscale eddy activity. Both the Abundance Index and sampling effort peaked in spring and summer, with a marked decline during winter. The influence of restricting the analysis period to March–November on the statistical significance of Abundance Index differences between AE and CE cores was assessed to account for uneven sample distribution, with results summarized in Table S1. Significant differences between AE and CE cores were observed in the southern (35°N–45°N) and northern (55°N–70°N) zones during March–August, whereas the middle zone (45°N–55°N) showed significant differences from April to October (Table S1).

3.4. The zooplankton Abundance Index varying with eddy radius

The Abundance Index varied significantly with eddy radius (Fig. 5a–c). Across eddy polarities, values within CE boundaries were significantly higher than those within AE boundaries in both the southern and northern zones ($Rr < 1$, $p < 0.05$; Fig. 5a and c), whereas no significant differences were observed outside eddy boundaries ($Rr > 1$). In contrast, within the middle zone, the Abundance Index tended to be higher within AE boundaries than within CE boundaries (Fig. 5b), with this pattern becoming more pronounced from April to October (Fig. S1a).

When comparing the Abundance Index inside versus outside eddy boundaries of the same polarity, anticyclonic eddies (AEs) in the southern and northern zones exhibited lower values within the eddy interiors relative to the surrounding waters, whereas cyclonic eddies (CEs) showed higher interior values (Fig. 5a and c). In contrast, eddies in the middle zone displayed the opposite pattern, with higher Abundance Index values within AEs and lower values within CEs (Fig. 5b, S1a).

The N:D values, representing the ratio of nighttime to daytime Abundance Index, exhibit clear latitudinal variability in relation to both eddy polarity and eddy region (Fig. 5d–f). In the northern zone, daytime and nighttime Abundance Index values are comparable, as indicated by overlapping standard error bars (Fig. 5f). In contrast, both the southern and middle zones show higher nighttime values, yielding N:D ratios greater than 1 (Fig. 5d and e). In the southern zone, the highest N:D ratio occur within CE cores, followed by the AE cores and then outside eddies. In the middle zone, the highest N:D ratio occurs within the AE core, followed by outside eddies and then CE cores.

3.5. Temporal variation of Abundance Index influenced by eddies

From 1993 to 2017, the zooplankton Abundance Index response to mesoscale eddies demonstrated clear temporal variability. Fig. 6a presents interannual trends for eddy cores, eddy edges, and non-eddy regions within the latitudinal range of 35°N to 70°N. Between 1993 and 2005, a slight decline was observed across all eddy regions, with an average slope of $k = -0.09\ \mathrm{yr}^{-1}$. In contrast, 2005–2017 revealed a significant increase, with an average slope of $k = 0.29\ \mathrm{yr}^{-1}$ ($p < 0.01$).

From 1993 to 2005, CE cores had significantly higher Abundance Index values than AE cores, whereas AE edges exceeded CE edges (Fig. 6a_1, 6a_2, $p < 0.01$). By contrast, from 2005 to 2017, differences between AE and CE were no longer statistically significant for either eddy cores or eddy edges.

Fig. 6b depicts temporal variations in the Abundance Index across three latitudinal bands, specifically within eddy cores and outside eddies, both of which exhibited broadly similar long-term trends. Notably, the patterns of variation differed among latitudinal zones. In the southern zone, the Abundance Index decreased from 1993 to 2005, followed by an increase from 2005 to 2017 (Fig. 6b_1). The middle zone showed a trend (Fig. 6b_2) consistent with the overall 35°N–70°N (Fig. 6a), likely reflecting the greater number of CPR observations in this zone (Fig. 4). In the northern zone, the Abundance Index generally increased from 1993 to 2010, followed by a decreasing trend from 2010 to 2017 (Fig. 6b_3).

Comparisons of the Abundance Index between eddy polarities revealed distinct latitudinal patterns (Fig. 6b). In the southern zone, the difference between AE and CE cores gradually diminished from 1993 to 2005 and became negligible thereafter (Fig. 6b_1), suggesting a weakened modulation effect of eddies over time. In the middle zone, the Abundance Index remained roughly comparable between AE and CE

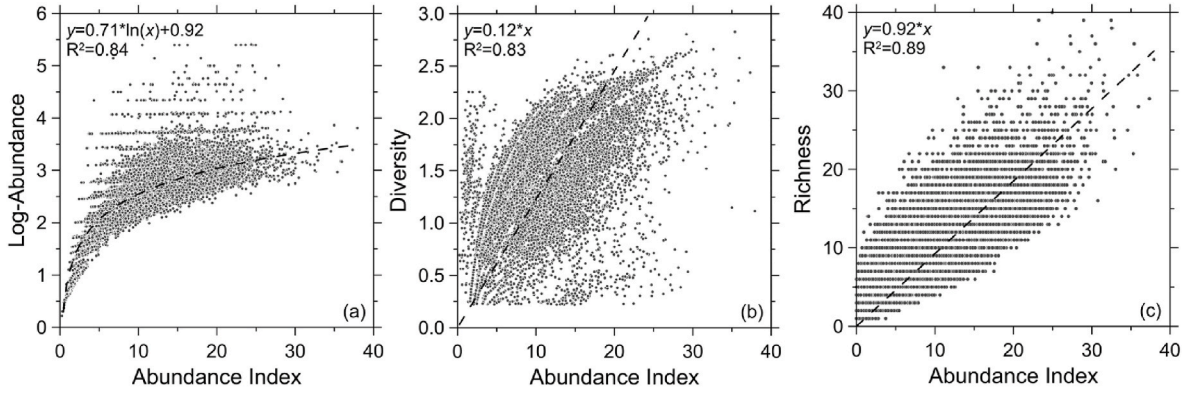

Fig. 3. Relationships between the Abundance Index and (a) total abundance, (b) diversity, and (c) richness. Scatter plots represent CPR-derived observations, while dashed lines represent the best-fit regression curves. R^2 indicates the coefficient of determination for each fitted model.

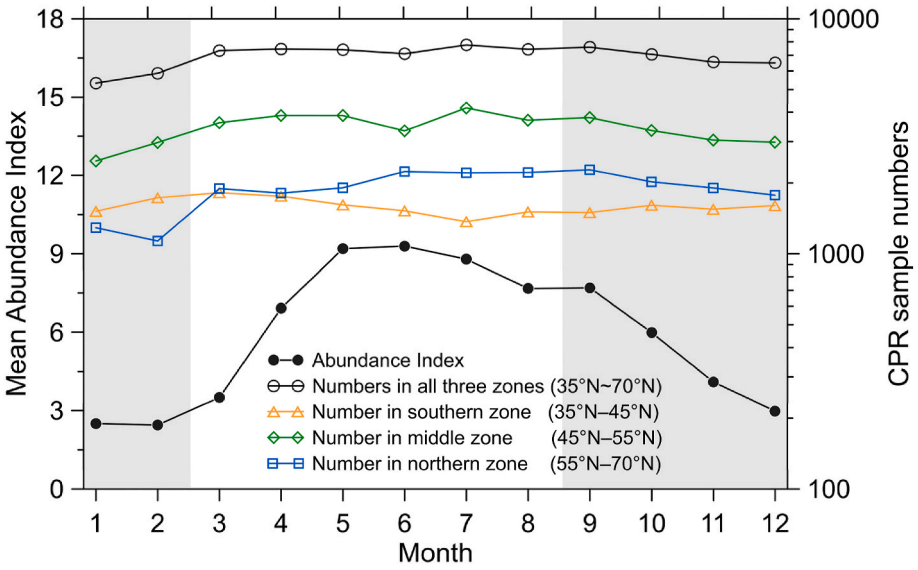

Fig. 4. Monthly variations in sample numbers across three latitudinal zones, alongside the mean Abundance Index over the entire region. Sample numbers remained relatively stable from March to August.

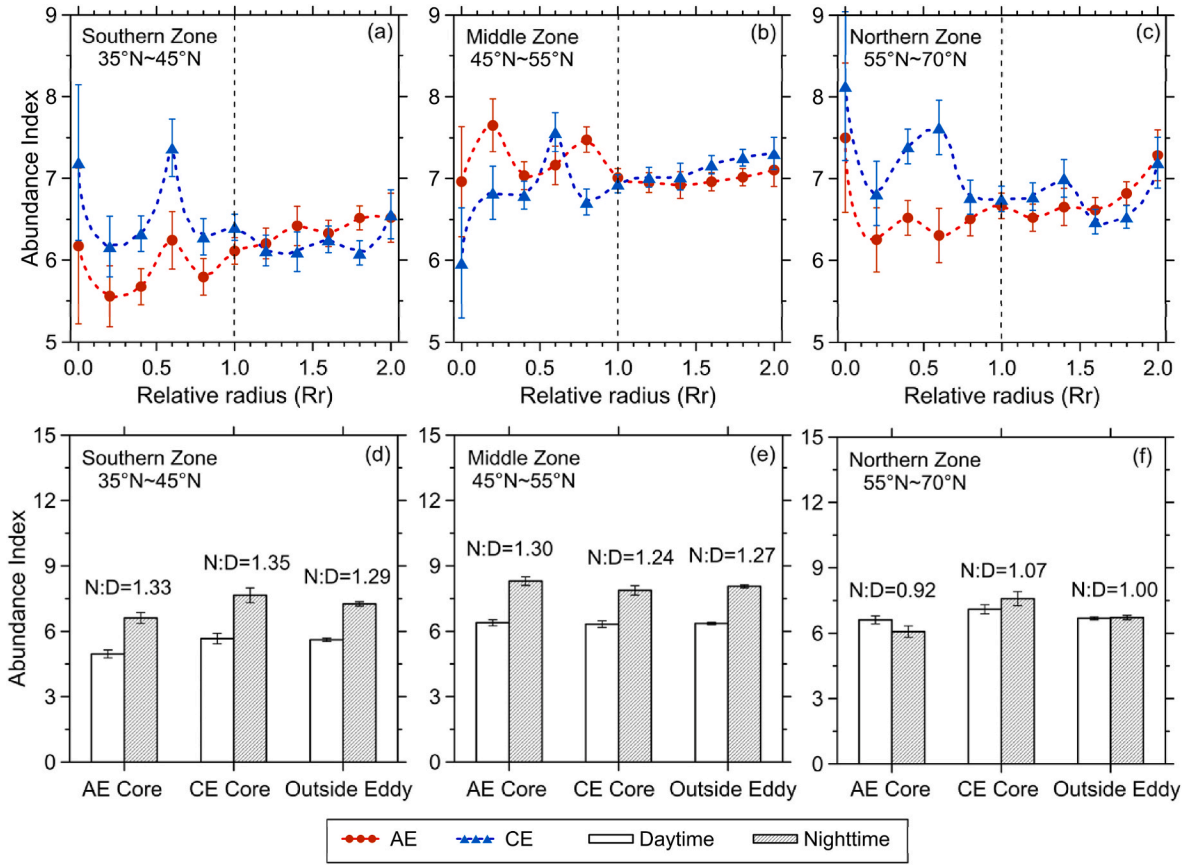

Fig. 5. Variations in the Abundance Index associated with eddies. (a) to (c) Abundance Index of AE and CE with eddy relative radius (*Rr*). (d) to (f) Abundance Index during daytime and nighttime across AE cores, CE cores (both $Rr < 0.8$), and outside eddies ($Rr > 1.2$). The vertical bars represent one standard error. N:D values indicate the ratio of nighttime to daytime.

cores from 1993 to 2003, but AE cores exhibited higher values in the subsequent years (Fig. 6b$_2$). By contrast, the northern zone consistently showed higher Abundance Index values in CE cores relative to AE cores, except between 2005 and 2008 (Fig. 6b$_3$).

Abundance Index anomalies offered a more nuanced view of the contrasting responses of zooplankton to AEs and CEs (Fig. 6c). From 1993 to 2017, anomaly values were significantly higher within CE cores compared with AE cores in both the southern and northern zones (Fig. 6c$_1$, 6c$_3$, $p < 0.001$). In contrast, from 2004 onwards, the middle zone exhibited significantly greater anomalies within AE cores than

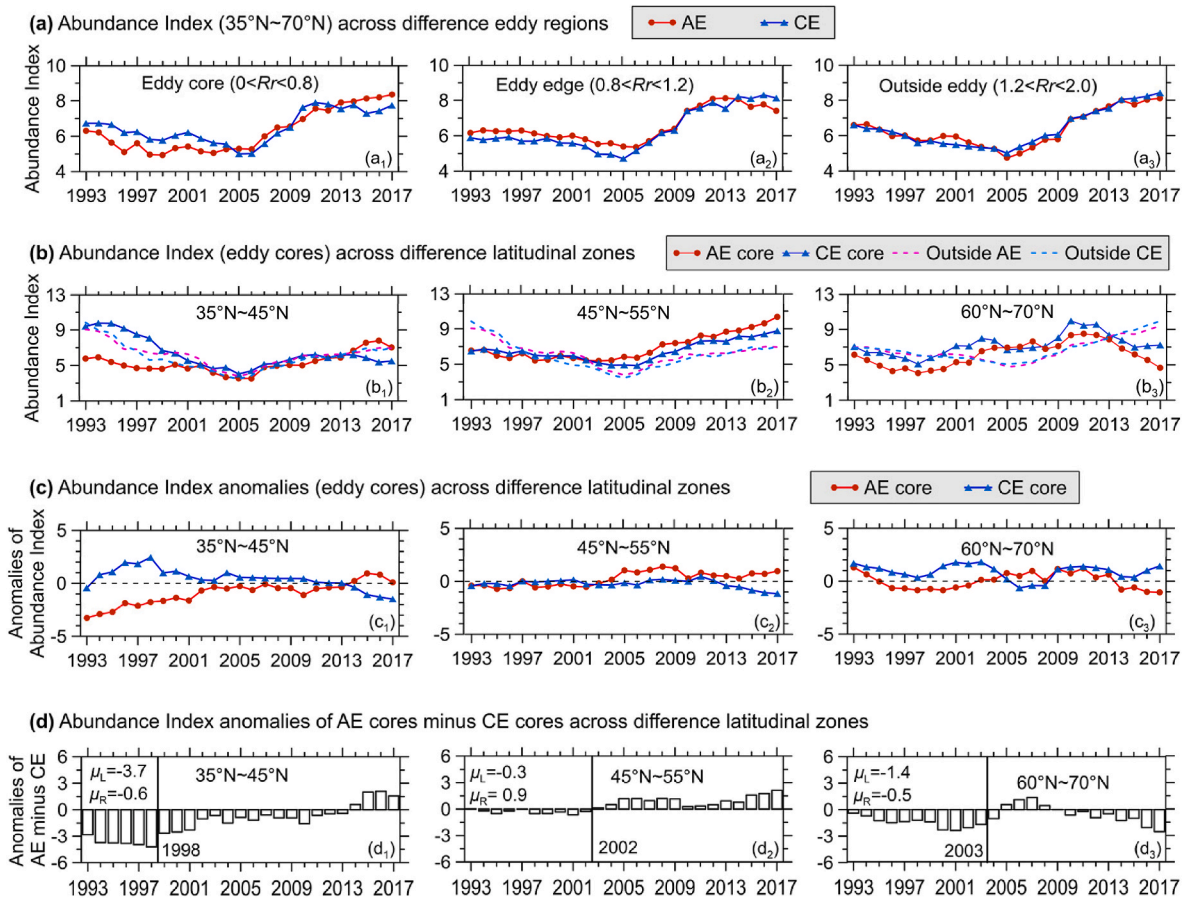

Fig. 6. Temporal variations in Abundance Index and its anomalies associated with eddies. Observations span from March to August during the period from January 01, 1998 to December 31, 2017. The time series were smoothed using a running average filter with a window size of 5 years.

within CE cores (Fig. 6c$_2$, $p < 0.05$).

Fig. 6d presents the temporal variations in anomaly differences (AE minus CE), underscoring the temporal variability of eddy polarity effects on zooplankton response. A sequential two-sample *t*-test identified statistically significant change points in the time series ($p < 0.001$), marking shifts in mean Abundance Index values before and after these points. Specifically, a significant shift occurred in 1998 for the southern zone ($p < 0.01$), in 2002 for the middle zone ($p < 0.01$), and in 2003 for the northern zone ($p < 0.05$). These shifts indicate a decline in the Abundance Index advantage within CE cores beginning in 1998 for the southern zone and in 2003 for the northern zone (Fig. 6d$_1$, 6d$_3$). Conversely, the middle zone demonstrated an increasing Abundance Index advantage within AE cores after 2002 (Fig. 6d$_2$).

3.6. Zooplankton variations with SST and Chl

Linear relationships between the Abundance Index and log-Chl are presented in Fig. 7. Significant positive correlations were observed, with the strongest associations found in the northern zone. In the southern zone, AE cores generally exhibited higher Abundance Index than CE cores under low Chl conditions, whereas CE cores exceeded those of AE cores at higher Chl levels (Fig. 7a). The middle zone displayed the opposite pattern: AE cores showed higher Abundance Index than CE cores when log-Chl exceeded a threshold value of −0.65 (Fig. 7b). In contrast, the northern zone consistently displayed higher Abundance Index within CE cores across all log-Chl ranges (Fig. 7c).

The relationships between the Abundance Index and SST exhibited multiple peaks across all latitudinal zones, but overall linear associations were weak (Fig. 7d–f). Specifically, a slight negative correlation was observed in the southern zone, a positive correlation emerged in the northern zone, whereas no significant relationship was detected between SST and the Abundance Index in the middle zone.

3.7. Effect of Chl and SST on zooplankton abundance

The contributions of these factors were assessed separately for AE cores, CE cores, and outside eddies (Fig. 8). *Feature Importance* (*FI*) values outside eddies remained relatively stable across the three latitudinal zones, with FI_{Chl} around 0.55 and FI_{SST} around 0.45. Within eddy cores, FI_{Chl} generally exceeded FI_{SST} across all regions, except for the AE core of the southern zone, where FI_{SST} was the higher value. In most cases, *FI* values within eddy cores differed from those outside eddies.

4. Discussion

Our analyses demonstrate distinct spatial patterns in zooplankton community responses to mesoscale eddies, with eddy polarity exerting contrasting effects across latitudinal zones. In addition to these spatial differences, long-term records reveal clear temporal shifts, including a pronounced post-2005 increase in the Abundance Index in the middle zone, as well as significant regime shifts detected in all three zones at different times. Together, these results highlight the importance of considering both spatial heterogeneity and temporal variability when evaluating eddy–zooplankton interactions. In the following discussion, we examine the mechanisms underlying these patterns and their broader ecological and climatic implications.

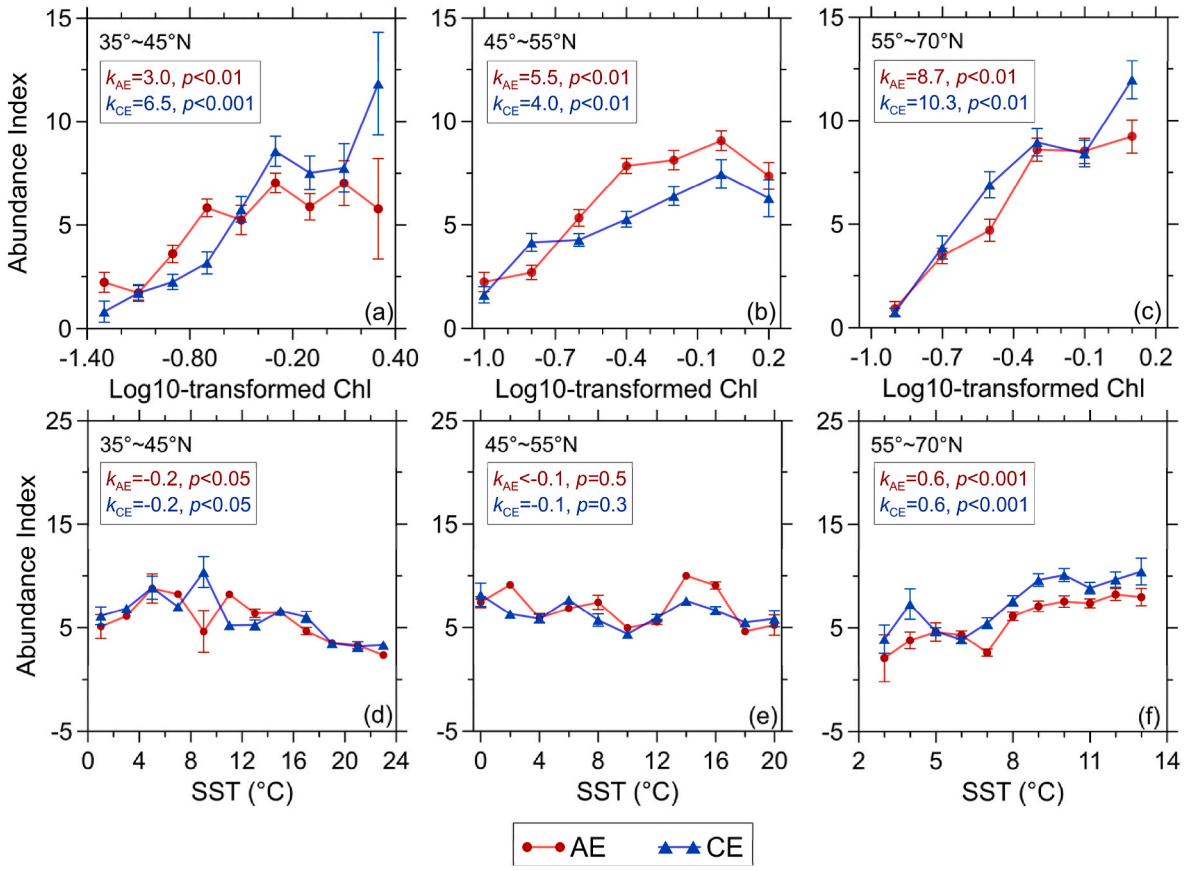

Fig. 7. Variability in Abundance Index in response to log-Chl and SST. The vertical bars indicate ±1 standard error. The slopes (k) and significance levels (p) of linear fits are labeled.

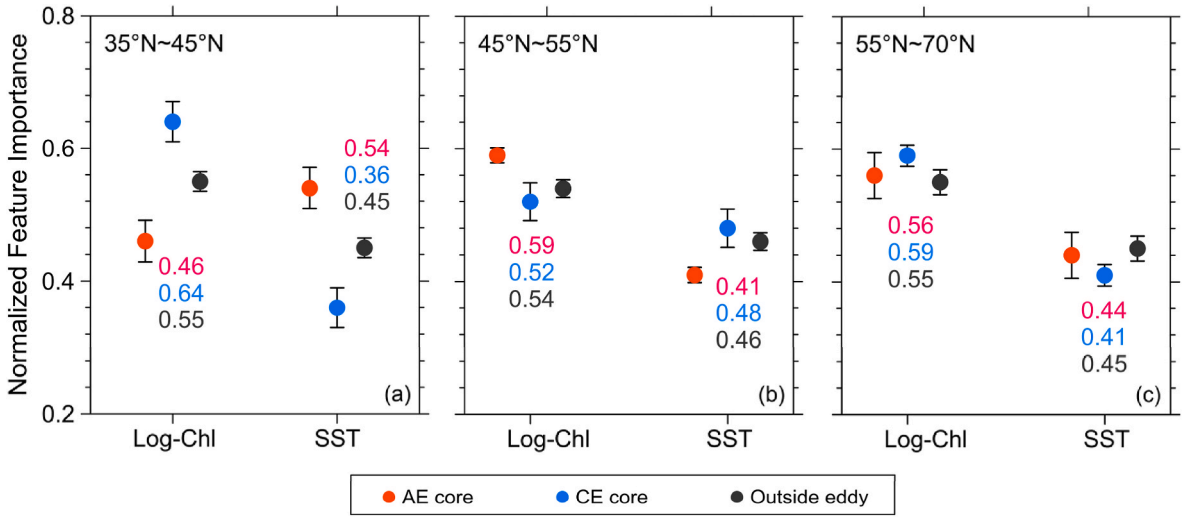

Fig. 8. Normalized *FI* of log-Chl and SST across the southern, middle and northern latitudinal zones. The *FI* of AE cores, CE cores, and outside eddies are plotted in red, blue, and black, respectively. The vertical bar indicates ±1 standard error. (For interpretation of the references to colour in this figure legend, the reader is referred to the Web version of this article.)

4.1. Method evaluation: The Abundance Index method

We developed an Abundance Index that integrates both numerical abundance and taxonomic diversity to quantify zooplankton responses to mesoscale eddies. Although a similar approach has previously been applied to examine long-term mesozooplankton changes in the southern North Sea, the Abundance Index in that context was neither clearly defined nor systematically (Di Pane et al., 2024). The strong correlations observed between the Abundance Index and well-established ecological metrics—log-transformed abundance ($r = 0.93$), richness ($r = 0.86$), and diversity ($r = 0.76$)—suggest that this Index effectively captures both numerical dominance and taxonomic breadth within zooplankton communities. By contrast, log-transformed abundance alone exhibited weaker correlations with richness ($r = 0.64$) and diversity ($r = 0.55$),

underscoring its limitation in reflecting community complexity. This demonstrates the utility of the Abundance Index in multi-taxa assemblages, where both the number of individuals and the number of taxa are ecologically relevant. Future work should evaluate the performance of this integrative index across different environmental conditions and assess whether it provides greater sensitivity in detecting shifts in community structure compared with conventional metrics.

The CPR dataset underscores a fundamental challenge in zooplankton monitoring: methodological differences in counting approaches can strongly shape perceived community patterns. Traverse-counted taxa typically dominate the raw counts (approximately 25 times more abundant than Eye-counted taxa), which may obscure ecologically meaningful signals from less abundant Eye-counted taxa. Such imbalances can bias interpretations of community responses to eddy dynamics if unadjusted metrics are employed (data not shown). In contrast, the Abundance Index offers a more balanced representation, reducing the disproportionate influence of highly abundant groups and providing a clearer link to mesoscale features such as eddy radius (Fig. 5). These findings suggest that integrative indices may outperform simple abundance transformations in detecting subtle ecological gradients, while also capturing the contributions of both dominant and rare taxa in community-level analyses.

4.2. Zooplankton responses to eddies: Long-term variability

Similar long-term trends observed across eddy cores, eddy edges, and regions outside eddies indicate that changes in the zooplankton Abundance Index are primarily driven by large-scale background environmental variability, rather than mesoscale processes alone (Fig. 6). Using a comparable approach, Pershing and Kemberling (2024) reported similar increases in two species after 2004. Likewise, Buttay et al. (2016) documented a decline in total zooplankton abundance on the Northwest Iberian Shelf from 1995 to 2003, followed by an increase from 2004 to 2010, consistent with our observations. One potential driver is the North Atlantic Oscillation (NAO), a dominant mode of large-scale atmospheric variability known to affect temperature (Hurrell, 1995), wind patterns, and consequently waves (Feng et al., 2014), as well as regional precipitation (Kyte et al., 2006), thereby influencing ocean mixing and stratification across the North Atlantic (Planque and Taylor, 1998). The influence of NAO on interannual zooplankton variability has been well documented, with positive NAO phases often associated with warmer temperatures and higher abundance (Piontkovski et al., 2006).

However, ecological responses to the NAO are spatially heterogeneous across the North Atlantic (Piontkovski et al., 2006; Ottersen et al., 2001), potentially leading to region-specific relationships. In the northern zone, the observed negative correlation between the NAO index and the difference in Abundance Index anomalies (Fig. 9; $r = -0.49$, $p < 0.02$), together with its strong associations with SST ($r = -0.81$, $p < 0.01$) and log-Chl ($r = -0.52$, $p < 0.01$), suggests that large-scale atmospheric variability may modulate zooplankton responses to eddy dynamics by altering temperature and primary productivity. In contrast, the weaker correlations observed in other regions underscore the need for further investigation to elucidate the mechanisms driving these spatial differences.

4.3. Eddy impacts on zooplankton: Underlying mechanisms

In the mid-latitude North Atlantic, our results indicate that zooplankton community responses to mesoscale eddies are spatially heterogeneous. This variability reflects the combined influence of eddy polarity (Sarmiento-Lezcano et al., 2024), eddy regions (Durán-Campos et al., 2015, 2019), and latitudinal zonation, factors that have also been shown to shape the foraging and distribution patterns of higher-trophic-level predators (Arostegui et al., 2022; Xing et al., 2024). The unique physical and ecological conditions formed within eddies, arising from their intrinsic dynamics, can modulate zooplankton distributions relative to surrounding waters (Rakhesh et al., 2008; Strzelecki et al., 2007).

One of the primary mechanisms governing zooplankton responses to mesoscale eddies is horizontal eddy trapping. During eddy formation, an eddy can entrain surrounding water masses along with their associated plankton communities, subsequently transporting them over substantial distances as they propagate (Mackas et al., 2005; McGillicuddy, 2016; Strzelecki et al., 2007). This physical isolation often generates distinct biogeochemical conditions within the eddy, setting it apart from surrounding waters. Such trapping effects are particularly pronounced in eddies formed within western and eastern boundary current systems (Gaube et al., 2014). Through this mechanism, elevated Chl concentrations entrained within the eddy indicate enhanced phytoplankton concentration, thereby creating more favorable conditions for zooplankton survival and growth. Thus, the eddy trapping effect extends beyond phytoplankton to include zooplankton. Observational studies have reported the concurrent presence of both coastal and offshore zooplankton species within a single eddy (Mackas et al., 2005). Similarly, Agulhas Rings drifting into the Atlantic Ocean retain species characteristics of the Indian Ocean (Cesar-Ribeiro et al., 2020), illustrating that mesoscale eddies can facilitate the redistribution of diverse plankton communities across oceanic regions.

In the mid-latitude North Atlantic, eddy pumping constitutes a key process influencing the vertical water properties within mesoscale eddies (Han et al., 2024). In CEs, it drives upwelling that brings nutrient-rich waters from depth into the euphotic zone (McGillicuddy and Robinson, 1997), thereby enhancing phytoplankton growth and primary production (McGillicuddy, 2016). This nutrient enrichment provides abundant food resources for zooplankton. It is widely recognized as a major physical-biological mechanism underpinning the

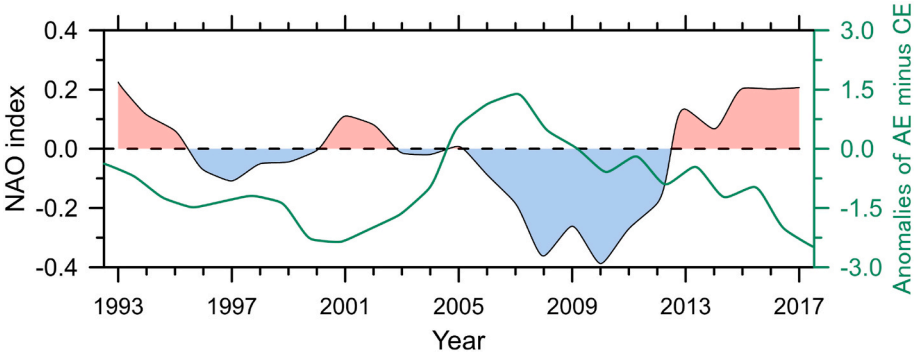

Fig. 9. NAO index and its correlations with differences of Abundance Index anomalies (AE minus CE) in the northern zone. The shaded areas indicate the NAO index smoothed with a 5-year running mean, to reveal the multi-annual variations. The green line indicates differences in Abundance Index anomalies. (For interpretation of the references to colour in this figure legend, the reader is referred to the Web version of this article.)

frequently observed zooplankton enrichment within CE interiors (Eden et al., 2009; Xiu and Chai, 2011).

In contrast, the eddy pumping mechanism induces downwelling within AEs, pushing warm, nutrient-poor surface waters to deeper layers (McGillicuddy, 2016). This vertical transport leads to elevated SST and reduced Chl concentrations near the eddy interior (Fig. S5). Notably, despite lower Chl levels relative to CEs, our analysis indicates elevated Abundance Index values within AEs in the middle zone. Similar patterns of increased zooplankton abundance or biomass in AEs have been documented in previous studies (Durán-Campos et al., 2019; Wang et al., 2023; Yebra et al., 2005). Comparable processes have been reported in Agulhas Rings, where strong vertical mixing transports nitrate from deeper waters into the euphotic zone, stimulating phytoplankton blooms that in turn support elevated zooplankton abundance and diversity (Cesar-Ribeiro et al., 2020; Villar et al., 2015).

Two additional mechanisms may also contribute:

(1) *Enhanced DVM:* Zooplankton within AEs may perform more active diel vertical migration (Wang et al., 2023; Yebra et al., 2005), promoting greater nighttime aggregation near the surface, thereby leading to higher surface abundances. This interpretation is supported by our findings (Fig. 5e), which indicate stronger DVM within AEs in the middle zone.
(2) *Thermal suitability:* AEs may offer more favorable thermal conditions that facilitate zooplankton growth and reproduction (Wang et al., 2023; Belkin et al., 2022; Yebra et al., 2005), thereby increasing abundance even under comparable Chl levels (Fig. 7b and e). These findings suggest that the interplay between behavioral and physiological processes can amplify zooplankton responses in anticyclonic systems, indicating that food availability alone is insufficient to fully determine zooplankton patterns.

4.4. The driven hypothesis: Food vs. temperature

Temperature and food availability (represented by Chl concentration) are recognized as key environmental drivers of zooplankton behavior (Fanjul et al., 2018; Tao et al., 2025). The pronounced latitudinal variability in zooplankton responses to mesoscale eddies prompted an examination of the relative contributions of these factors across different zones. We initially considered that temperature might play a larger role in the middle zone, given that zooplankton aggregated within AE cores despite the relatively low Chl concentrations (Fig. 5, S5). However, the patterns in Fig. 8 suggest that the food-driven hypothesis offers a more consistent explanation for zooplankton distributions across the broader latitudinal range. This interpretation is further supported by the patterns derived from Fig. 5, which suggest that DVM may partially account for the slightly higher zooplankton abundance observed in AE cores relative to CE cores in the middle zone (Annasawmy et al., 2024; Liu et al., 2020). Notably, in the northern zone, where Chl concentrations are generally high, food availability appears to exert a strong influence on zooplankton distributions (Eden et al., 2009). The consistently higher abundance within CE cores compared with AE cores across a range of Chl and SST levels further supports this interpretation (Fig. 7c and f).

A notable exception to the general latitudinal pattern was observed in the AE core of the southern zone, where the temperature-driven hypothesis is somewhat better supported (Vortmeyer-Kley et al., 2019; Wang et al., 2023). We suggest that this anomaly may arise from the combined effects of two interacting mechanisms. First, the strong negative correlation observed between SST and the Abundance Index in the southern zone indicates that zooplankton within AEs may be particularly sensitive to elevated temperatures. Second, this response may be influenced by elevated predation pressure. AE-induced downwelling transports warmer, oxygenated waters downward, potentially facilitating the aggregation of higher-trophic-level predators, such as squid and fish (Arostegui et al., 2022; Xing et al., 2024). These physical and biogeochemical anomalies associated with AEs may indirectly suppress zooplankton abundance through intensified predation. This hypothesis is partially corroborated by the pattern observed in Fig. 7a, where the Abundance Index within AEs stabilizes as log-Chl rises to 0, contrasting with the continuous increase observed in CEs and highlighting a pronounced divergence between the two eddy types.

4.5. Caveats

Several limitations should be considered when interpreting our findings. First, methodological aspects of the CPR survey could have influenced the results. Over its operational history, the CPR progressively incorporated additional taxa into its counts, most notably around 2004, when approximately 10 phytoplankton and 4 zooplankton taxa were added (Richardson et al., 2006). Despite this, neither the annual number of recorded zooplankton taxa nor the unsmoothed Abundance Index indicated abrupt changes in 2004 (Fig. S4). Statistical analysis further indicates that the four newly adjusted taxonomic groups in 2004 (*Acantharia*, *Foraminifera**, *Radiolaria** and *Heterophryxus appendiculatus*) together accounted for only ~4 % of the Abundance Index. Given their relatively minor contribution, the trend shift detected in that year (Fig. 6a) is unlikely to be primarily attributable to methodological artifacts. Similar expansions in recorded taxa occurred around 1996 and 2008, followed by stabilization, and these changes appear to have minimal impact on the overall upward trend in zooplankton abundance. Collectively, these observations suggest that methodological changes in the CPR survey exerted limited influence on the major patterns reported here.

Another limitation arises from differences in sampling depth across datasets, which may weaken the observed correlations. The CPR primarily samples at ~7 m. In contrast, satellite-derived SST reflects the surface skin layer, Chl concentrations represent an integrated value over the optical depth, and peak zooplankton abundance often occurs below 50 m (Ashjian et al., 2004; Forest et al., 2012).

A further issue cencerns the relatively short 25-year duration of satellite-derived datasets, which constrains the detection of long-term variability and limits both the validation of identified shift points and the assessment of basin-scale climatic drivers. Extending observational records over longer timescales will be essential to confirm these patterns and to elucidate the mechanisms underlying long-term ecosystem changes.

In addition, the present analysis does not explicitly account for biological heterogeneity among species and size classes. Incorporating such variability in future work will be crucial for advancing our understanding of taxon- and size-specific zooplankton responses to mesoscale dynamics.

5. Conclusion

This study introduces a novel Abundance Index that integrates both abundance and richness, offering a more balanced representation of zooplankton community structure compared with traditional single-metric approaches. By applying this metric to a 25-year CPR dataset in the mid-latitude North Atlantic, we identified distinct and spatially heterogeneous zooplankton responses to mesoscale eddies. Specifically, zooplankton enrichment was generally associated with CEs through nutrient-driven phytoplankton enhancement, whereas aggregation within anticyclonic eddies appeared more strongly linked to thermal suitability and enhanced DVM. Our results further emphasize that food availability, rather than temperature, is a more influential factor driving zooplankton community responses across latitudinal zones, particularly in the northern zone.

Long-term analyses further revealed a pronounced increase in the Abundance Index in the middle latitudinal zone after 2005, and this increase was accompanied by significant temporal shifts in how eddy

polarity influenced zooplankton. Specifically, change points identified in 1998 and 2003 indicate a weakening of the Abundance Index advantage within CE cores in the southern and northern zones, whereas the middle zone exhibited a growing advantage within AE cores after 2002. Together, these findings underscore that eddy–zooplankton interactions cannot be fully understood without considering temporal variability and large-scale climatic forcing.

Collectively, our results advance mechanistic understanding of how mesoscale physical processes interact with ecological drivers to shape zooplankton communities. The Abundance Index provides a sensitive tool for detecting ecological responses to both mesoscale and large-scale variability, with promising applications for ecosystem monitoring and forecasting under future climate change scenarios.

CRediT authorship contribution statement

Guiyan Han: Writing – review & editing, Writing – original draft, Software, Methodology, Investigation, Formal analysis, Conceptualization. **Graham D. Quartly:** Writing – review & editing, Writing – original draft, Validation, Supervision, Methodology, Investigation, Funding acquisition, Formal analysis. **Hui Wang:** Writing – review & editing, Supervision, Investigation, Funding acquisition. **Jie Yang:** Writing – review & editing, Validation, Investigation. **Ge Chen:** Writing – review & editing, Supervision, Investigation, Funding acquisition, Conceptualization.

Data statement

The zooplankton observations from the CPR survey are distributed by MBA and are available at https://www.dassh.ac.uk/ipt/resource?r=cpr_public.

For satellite products, the sea level anomalies dataset (1993–2017) distributed by AVISO can be accessed at https://resources.marine.copernicus.eu/products.

The mesoscale eddy dataset (1993–2017) produced by Tian et al. (2020) is public at https://data.casearth.cn/en/sdo/detail/5fa668ad1f4600005e005ba3.

The chlorophyll product (1998–2017) is distributed by the GlobColour project at https://hermes.acri.fr/.

Sea surface temperature product (OI SST V2, 1993–2017) distributed by NOAA Physical Sciences Laboratory are available at https://psl.noaa.gov/data/gridded/data.noaa.oisst.v2.highres.html.

Declaration of competing interest

The authors declare that they have no known competing financial interests or personal relationships that could have appeared to influence the work reported in this paper.

Acknowledgement

This research was jointly supported by the National Natural Science Foundation of China (Grant No. 42530404), the China Postdoctoral Science Foundation (Grant No. 2025M770329), and the research time of Graham D. Quartly was supported by the NERC Centre for Earth Observation (NCEO). We are very grateful to the China Scholarship Council for its support for the academic visiting of Guiyan Han to at Plymouth Marine Laboratory. We appreciated comments from Liz Atwood, Giorgio Dall'Olmo, and Angus Atkinson on a draft version of this paper, and are very grateful to David Johns, Stephanie Allen and Angus Atkinson for their help with the CPR project data.

Appendix A. Supplementary data

Supplementary data to this article can be found online at https://doi.org/10.1016/j.dsr.2025.104605.

Data availability

The data is publicly available and is described in the Data Statement.

References

An, L.N., Liu, X., Xu, F.P., Fan, X.Y., Wang, P.X., Yin, W.F., Huang, B.Q., 2024. Different responses of plankton community to mesoscale eddies in the western equatorial Pacific Ocean. Deep-Sea Res Pt I 203, 104219. https://doi.org/10.1016/j.dsr.2023.104219.

Annasawmy, P., Roudaut, G., Lebourges Dhaussy, A., 2024. Impact of an eddy dipole of the Mozambique channel on mesopelagic organisms, highlighted by multifrequency backscatter classification. Plots One 19 (9), e0309840. https://doi.org/10.1371/journal.pone.0309840.

Arostegui, M.C., Gaube, P., Woodworth-Jefcoats, P.A., Kobayashi, D.R., Braun, C.D., 2022. Anticyclonic eddies aggregate pelagic predators in a subtropical gyre. Nature 609, 535–540. https://doi.org/10.1038/s41586-022-05162-6.

Ashjian, C.J., Rosenwaks, G.A., Wiebe, P.H., Davis, C.S., Gallager, S.M., Copley, N.J., Lawson, G.L., Alatalo, P., 2004. Distribution of zooplankton on the continental shelf off marguerite Bay, antarctic peninsula, during Austral fall and winter, 2001. Deep-Sea Res Pt Ii 51, 2073–2098. https://doi.org/10.1016/j.dsr2.2004.07.025.

AVISO, 2019. SSALTO/DUACS User Handbook: (M)SLA and (M)ADT near-real Time and Delayed Time Products, 2019, Issue 5.0, AVISO Publ, CLS-DOS-NT-06-034, SALP-MU-PEA-21065-CLS [M].

Batten, S.D., Crawford, W.R., 2005. The influence of coastal origin eddies on oceanic plankton distributions in the eastern Gulf of Alaska. Deep-Sea Res Pt Ii 52, 991–1009. https://doi.org/10.1016/j.dsr2.2005.02.009.

Behrenfeld, M.J., Gaube, P., Della Penna, A., O'Malley, R.T., Burt, W.J., Hu, Y., Bontempi, P.S., Steinberg, D.K., Boss, E.S., Siegel, D.A., Hostetler, C.A., Tortell, P.D., Doney, S.C., 2019. Global satellite-observed daily vertical migrations of ocean animals. Nature 576, 257–261. https://doi.org/10.1038/s41586-019-1796-9.

Belkin, N., Guy-Haim, T., Rubin-Blum, M., Lazar, A., Sisma-Ventura, G., Kiko, R., Morov, A.R., Ozer, T., Gertman, I., Herut, B., Rahav, E., 2022. Influence of cyclonic and anticyclonic eddies on plankton in the southeastern Mediterranean Sea during late summertime. Ocean Sci. 18, 693–715. https://doi.org/10.5194/os-18-693-2022.

Benedetti, F., Vogt, M., Elizondo, U.H., Righetti, D., Zimmermann, N.E., Gruber, N., 2021. Major restructuring of marine plankton assemblages under global warming. Nat. Commun. 12, 5226. https://doi.org/10.1038/s41467-021-25385-x.

Buttay, L., Miranda, A., Casas, G., González - quirós, R., Nogueira, E., 2016. Long-term and seasonal zooplankton dynamics in the northwest Iberian shelf and its relationship with meteo-climatic and hydrographic variability. J. Plankton Res. 38 (1), 106–121. https://doi.org/10.1093/plankt/fbv100.

Campbell, J.W., 1995. The lognormal distribution as a model for bio-optical variability in the sea. J. Geophys Res-Oceans 100, 13237–13254. https://doi.org/10.1029/95JC00458.

Cesar-Ribeiro, C., Piedras, F.R., da Cunha, L.C., de Lima, D.T., Pinho, L.Q., Moser, G.A.O., 2020. Is oligotrophy an equalizing factor driving microplankton species functional diversity within agulhas rings? Front. Mar. Sci. 7. https://doi.org/10.3389/fmars.2020.599185.

Chelton, D.B., Gaube, P., Schlax, M.G., Early, J.J., Samelson, R.M., 2011a. The influence of nonlinear mesoscale eddies on near-surface oceanic chlorophyll. Science 334, 328–332. https://doi.org/10.1126/science.1208897.

Chelton, D.B., Schlax, M.G., Samelson, R.M., 2011b. Global observations of nonlinear mesoscale eddies. Prog. Oceanogr. 91, 167–216. https://doi.org/10.1016/j.pocean.2011.01.002.

Di Pane, J., Boersma, M., Marques, R., Deschamps, M., Ecker, U., Meunier, C.L., 2024. Identification of tipping years and shifts in mesozooplankton community structure using multivariate analyses: a long-term study in southern north sea. ICES J. Mar. Sci. 81, 553–563. https://doi.org/10.1093/icesjms/fsad071.

Durán-Campos, E., Monreal-Gómez, M.A., de León, D.A.S., Coria-Monter, E., 2019. Zooplankton functional groups in a dipole eddy in a coastal region of the southern gulf of California. Reg. Stud. Mar. Sci. 28, 100588. https://doi.org/10.1016/j.rsma.2019.100588.

Durán-Campos, E., Salas-de-León, D.A., Monreal-Gómez, M.A., Aldeco-Ramírez, J., Coria-Monter, E., 2015. Differential zooplankton aggregation due to relative vorticity in a semi-enclosed bay. Estuar. Coast Shelf Sci. 164, 10–18. https://doi.org/10.1016/j.ecss.2015.06.030.

Eden, B.R., Steinberg, D.K., Goldthwait, S.A., McGillicuddy, D.J., 2009. Zooplankton community structure in a cyclonic and mode-water eddy in the Sargasso Sea. Deep-Sea Res Pt I 56, 1757–1776. https://doi.org/10.1016/j.dsr.2009.05.005.

Falkowski, P.G., Ziemann, D., Kolber, Z., Bienfang, P.K., 1991. Role of eddy pumping in enhancing primary production in the ocean. Nature 352, 55–58. https://doi.org/10.1038/352055a0.

Fanjul, A., Iriarte, A., Villate, F., Uriarte, I., Atkinson, A., Cook, K., 2018. Zooplankton seasonality across a latitudinal gradient in the northeast Atlantic shelves province. Cont. Shelf Res. 160, 49–62. https://doi.org/10.1016/j.csr.2018.03.009.

Feng, X.B., Tsimplis, M.N., Yelland, M.J., Quartly, G.D., 2014. Changes in significant and maximum wave heights in the Norwegian Sea. Global Planet. Change 113, 68–76. https://doi.org/10.1016/j.gloplacha.2013.12.010.

Forest, A., Stemmann, L., Picheral, M., Burdorf, L., Robert, D., Fortier, L., Babin, M., 2012. Size distribution of particles and zooplankton across the shelf-basin system in southeast beaufort sea: combined results from an underwater vision profiler and

vertical net tows. Biogeosciences 9, 1301–1320. https://doi.org/10.5194/bg-9-1301-2012.
Gaube, P., Chelton, D.B., Samelson, R.M., Schlax, M.G., O'Neill, L.W., 2015. Satellite observations of mesoscale eddy-induced ekman pumping. J. Phys. Oceanogr. 45, 104–132. https://doi.org/10.1175/Jpo-D-14-0032.1.
Gaube, P., McGillicuddy, D.J., Chelton, D.B., Behrenfeld, M.J., Strutton, P.G., 2014. Regional variations in the influence of mesoscale eddies on near-surface chlorophyll. J. Geophys Res-Oceans 119, 8195–8220. https://doi.org/10.1002/2014jc010111.
Govoni, J.J., Hare, J.A., Davenport, E.D., Chen, M.H., Marancik, K.E., 2010. Mesoscale, cyclonic eddies as larval fish habitat along the southeast United States shelf: a Lagrangian description of the zooplankton community. ICES J. Mar. Sci. 67, 403–411. https://doi.org/10.1093/icesjms/fsp269.
Han, G.Y., Quartly, G.D., Chen, G., Yang, J., 2024. Satellite-observed SST and chlorophyll reveal contrasting dynamical-biological effects of mesoscale eddies in the north Atlantic. Environ. Res. Lett. 19, 104035. https://doi.org/10.1088/1748-9326/ad7049.
Hurrell, J.W., 1995. Decadal trends in the north Atlantic oscillation: regional temperatures and precipitation. Science 269, 676–679. https://doi.org/10.1126/science.269.5224.676.
Johns, D., Broughton, D., 2022. The CPR Survey. v1.3. Marine Biological Association. Dataset/Samplingevent. https://doi.org/10.17031/1629.
Kyte, E.A., Quartly, G.D., Srokosz, M.A., Tsimplis, M.N., 2006. Interannual variations in precipitation: the effect of the north Atlantic and southern oscillations as seen in a satellite precipitation data set and in models. J. Geophys. Res., [Atmos.] 111. https://doi.org/10.1029/2006jd007138.
Labat, J.P., Gasparini, S., Mousseau, L., Prieur, L., Boutoute, M., Mayzaud, P., 2009. Mesoscale distribution of zooplankton biomass in the northeast Atlantic Ocean determined with an optical plankton counter: relationships with environmental structures. Deep-Sea Res. Pt. I 56, 1742–1756. https://doi.org/10.1016/j.dsr.2009.05.013.
Liu, H.J., Zhu, M.L., Guo, S.J., Zhao, X.H., Sun, X.X., 2020. Effects of an anticyclonic eddy on the distribution and community structure of zooplankton in the South China Sea northern slope. J. Mar. Syst. 205, 103311. https://doi.org/10.1016/j.jmarsys.2020.103311.
Lu, Y., Zhang, Y., Wang, J.H., Zhang, M., Wu, Y., Xiao, X., Xu, J., 2022. Dynamics in bacterial community affected by mesoscale eddies in the northern slope of the South China Sea. Microb. Ecol. 83, 823–836. https://doi.org/10.1007/s00248-021-01816-6.
Mackas, D.L., Tsurumi, M., Galbraith, M.D., Yelland, D.R., 2005. Zooplankton distribution and dynamics in a north Pacific eddy of coastal origin: II. Mechanisms of eddy colonization by and retention of offshore species. Deep-Sea Res Pt Ii 52, 1011–1035. https://doi.org/10.1016/j.dsr2.2005.02.008.
McGillicuddy, D.J., 2016. Mechanisms of physical-biological-biogeochemical interaction at the Oceanic mesoscale. Ann. Rev. Mar. Sci 8, 125–159. https://doi.org/10.1146/annurev-marine-010814-015606.
McGillicuddy, D.J., Anderson, L.A., Bates, N.R., Bibby, T., Buesseler, K.O., Carlson, C.A., Davis, C.S., Ewart, C., Falkowski, P.G., Goldthwait, S.A., Hansell, D.A., Jenkins, W.J., Johnson, R., Kosnyrev, V.K., Ledwell, J.R., Li, Q.P., Siegel, D.A., Steinberg, D.K., 2007. Eddy/wind interactions stimulate extraordinary mid-ocean plankton blooms. Science 316, 1021–1026. https://doi.org/10.1126/science.1136256.
McGillicuddy, D.J., Robinson, A.R., 1997. Eddy-induced nutrient supply and new production in the Sargasso Sea. Deep-Sea Res Pt I 44 (8), 1427–1450. https://doi.org/10.1016/S0967-0637(97)00024-1.
Ottersen, G., Planque, B., Belgrano, A., Post, E., Reid, P.C., Stenseth, N.C., 2001. Ecological effects of the north Atlantic oscillation. Oecologia 128, 1–14. https://doi.org/10.1007/s004420100655.
Pershing, A.J., Kemberling, A., 2024. Decadal comparisons identify the drivers of persistent changes in the zooplankton community structure in the northwest Atlantic. ICES J. Mar. Sci. 81 (3), 564–574. https://doi.org/10.1093/icesjms/fsad198.
Piontkovski, S.A., O'brien, T.D., Umani, S.F., Krupa, E.G., Stuge, T.S., Balymbetov, K.S., Grishaeva, O.V., Kasymov, A.G., 2006. Zooplankton and the north Atlantic oscillation: a basin-scale analysis. J. Plankton Res. 28, 1039–1046. https://doi.org/10.1093/plankt/fbl037.
Piontkovski, S.A., Williams, R., Peterson, W., Kosnirev, V.K., 1995. Relationship between oceanic mesozooplankton and energy of eddy fields. Mar. Ecol. Prog. Ser. 128, 35–41. https://doi.org/10.3354/meps128035.
Planque, B., Taylor, A.H., 1998. Long-term changes in zooplankton and the climate of the north Atlantic. ICES J. Mar. Sci. 55, 644–654. https://doi.org/10.1006/jmsc.1998.0390.
Quartly, G.D., Legeais, J.F., Ablain, M., Zawadzki, L., Fernandes, M.J., Rudenko, S., Carrère, L., García, P.N., Cipollini, P., Andersen, O.B., Poisson, J.C., Njiche, S.M., Cazenave, A., Benveniste, J., 2017. A new phase in the production of quality-controlled sea level data. Earth Syst. Sci. Data 9, 557–572. https://doi.org/10.5194/essd-9-557-2017.
Rakhesh, M., Raman, A.V., Kalavati, C., Subramanian, B.R., Sharma, V.S., Babu, E.S., Sateesh, N., 2008. Zooplankton community structure across an eddy-generated upwelling band close to a tropical bay-mangrove ecosystem. Mar. Biol. 154, 953–972. https://doi.org/10.1007/s00227-008-0991-2.
Rettig, J.E., 2003. Zooplankton responses to predation by larval bluegill: an enclosure experiment. Freshw. Biol 48, 636–648. https://doi.org/10.1046/j.1365-2427.2003.01035.x.
Richardson, A.J., Walne, A.W., John, A.W.G., Jonas, T.D., Lindley, J.A., Sims, D.W., Stevens, D., Witt, M., 2006. Using continuous plankton recorder data. Prog. Oceanogr. 68, 27–74. https://doi.org/10.1016/j.pocean.2005.09.011.
Sarmiento-Lezcano, A.N., Aceves-Medina, G., Villalobos, H., Hernández-Trujillo, S., 2024. Composition and distribution of the zooplankton community along the west coast of Baja California peninsula and its relationships with the environment variables. J. Mar. Syst. 242, 103940. https://doi.org/10.1016/j.jmarsys.2023.103940.
Strzelecki, J., Koslow, J.A., Waite, A., 2007. Comparison of mesozooplankton communities from a pair of warm- and cold-core eddies off the coast of Western Australia. Deep-Sea Res Pt Ii 54, 1103–1112. https://doi.org/10.1016/j.dsr2.2007.02.004.
Tao, Z.C., Wang, S., Chi, X.P., Zhang, F., Sun, S., 2025. Zooplankton community structure and vertical distribution in the South China Sea during the summer monsoon. Mar. Pollut. Bull. 215, 117857. https://doi.org/10.1016/j.marpolbul.2025.117857.
Tian, F.L., Wu, D., Yuan, L.M., Chen, G., 2020. Impacts of the efficiencies of identification and tracking algorithms on the statistical properties of global mesoscale eddies using merged altimeter data. Int. J. Rem. Sens. 41, 2835–2860. https://doi.org/10.1080/01431161.2019.1694724.
Villar, E., Farrant, G.K., Follows, M., Garczarek, L., Speich, S., Audic, S., Iudicone, D., 2015. Environmental characteristics of Agulhas rings affect interocean plankton transport. Science 348 (6237), 1261447. https://doi.org/10.1126/science.1261447.
Vortmeyer-Kley, R., Lünsmann, B., Berthold, M., Gräwe, U., Feudel, U., 2019. Eddies: fluid dynamical niches or transporters?–A case study in the western Baltic sea. Front. Mar. Sci. 6. https://doi.org/10.3389/fmars.2019.00118.
Wang, Y., Zhang, J.H., Yu, J.C., Wu, Q.Y., Sun, D., 2023. Anticyclonic mesoscale eddy induced mesopelagic biomass hotspot in the oligotrophic ocean. J. Mar. Syst. 237. https://doi.org/10.1016/j.jmarsys.2022.103831.
Xing, Q.W., Yu, H.Q., Wang, H., Ito, S., Yu, W., 2024. Mesoscale eddies exert inverse latitudinal effects on global industrial squid fisheries. Sci. Total Environ. 950, 175211. https://doi.org/10.1016/j.scitotenv.2024.175211.
Xing, Q.W., Yu, H.Q., Wang, H., Ito, S.I., Chai, F., 2023. Mesoscale eddies modulate the dynamics of human fishing activities in the global midlatitude ocean. Fish Fish. 24, 527–543. https://doi.org/10.1111/faf.12742.
Xiu, P., Chai, F., 2011. Modeled biogeochemical responses to mesoscale eddies in the South China Sea. J. Geophys Res-Oceans 116. https://doi.org/10.1029/2010jc006800.
Xiu, P., Chai, F., 2020. Eddies affect subsurface phytoplankton and oxygen distributions in the North Pacific subtropical gyre. Geophys. Res. Lett. 47, e2020GL087037. https://doi.org/10.1029/2020GL087037.
Yebra, L., Almeida, C., Hernández-León, S., 2005. Vertical distribution of zooplankton and active flux across an anticyclonic eddy in the canary island waters. Deep-Sea Res Pt I 52, 69–83. https://doi.org/10.1016/j.dsr.2004.08.010.
Zhu, Y.W., Tande, K.S., Zhou, M., 2009. Mesoscale physical processes and zooplankton transport-retention in the northern Norwegian shelf region. Deep-Sea Res Pt Ii 56, 1922–1933. https://doi.org/10.1016/j.dsr2.2008.11.019.